Available online at www.sciencedirect.com
ScienceDirect
International Journal of Multiphase Flow 33 (2007) 510–524
International Journal of Multiphase Flow
www.elsevier.com/locate/ijmulflow

Coupling level set/VOF/ghost fluid methods: Validation and application to 3D simulation of the primary break-up of a liquid jet

T. Ménard [a], S. Tanguy [b], A. Berlemont [a,*]

[a] UMR6614-CORIA, Technopôle du Madrillet, BP 12 Avenue de l'Université, 76801 Saint-Etienne-du-Rouvray Cedex, France
[b] LEMTA CNRS UMR – 7563, 2, avenue de la forêt de Haye, BP 160, 54504 Vandoeuvre lès Nancy, France

Received 9 March 2006; received in revised form 23 October 2006

Abstract

Numerical simulations are carried out to describe the dense zone of a spray where very little information is available, either from experimental or theoretical approaches. Interface tracking is ensured by the level set method and the ghost fluid method (GFM) is used to capture accurately sharp discontinuities for pressure, density and viscosity. The level set method is coupled with the VOF method for mass conservation.

The level set–VOF coupling is validated on 2D and 3D test cases. The level set–ghost fluid method is applied to the Rayleigh instability of a liquid jet. Preliminary results are then presented for 3D simulation of the primary break-up of a turbulent liquid jet with the level set–VOF–ghost fluid method.

1. Introduction

Extensive studies have been devoted to the transport of droplet sprays, but the atomization process remains a challenging topic of research; DNS simulations provide a promising tool for obtaining information in the dense zone of the spray, where nearly no experimental data are available. But it clearly appears that specific approaches must be developed for the description of interface behavior. Computing interface motion in multiphase flows is a wide field of research and several approaches can be used. Front tracking methods (Unverdi and Tryggvason, 1992), Volume of fluid methods (Gueyffier et al., 1999) and level set methods (Sussman et al., 1994) are the most common numerical strategies used to predict interface motion. Front tracking methods are based on the Lagrangian tracking of marker particles that are attached to the interface motion, but appear numerically limited for 3D geometries, especially for the distribution of the marker particles when irregularities occur on the interface. Volume of fluid methods are based on the description of the volumetric fraction of each phase in grid cells. The main difficulty of the method is that 2D interface reconstruction is quite difficult,

* Corresponding author. Tel.: +33 2 32 95 36 17; fax: +33 2 32 91 04 85.
E-mail address: Alain.Berlemont@coria.fr (A. Berlemont).

0301-9322/$ - see front matter © 2006 Published by Elsevier Ltd.
doi:10.1016/j.ijmultiphaseflow.2006.11.001

and 3D reconstruction is numerically prohibitive. A consequence can be some uncertainties on the interface curvature and thus on the surface tension forces. The basis of the Level Set methods has been proposed by Osher and Sethian (1988); the interface is described with the zero level curve of a continuous function defined by the signed distance to the interface. To ensure that the function remains the signed distance to the interface, a redistancing algorithm is applied, but it is well known that its numerical computation can generate mass loss in under-resolved regions. This is the main drawback of level set methods. To describe the interface discontinuities, two approaches can be used, namely the continuous force formulation (''delta'' formulation), which assumes that the interface is 2 or 3 grid meshes thick, and the ghost fluid method (GFM), which has been derived by Fedkiw et al. (1999) to capture jump conditions on the interface. The GFM approach not only avoids the introduction of a fictitious interface thickness, but it is also suitable to provide a more accurate discretization of discontinuous terms, reducing parasitic currents and improving the resolution on the pressure jump condition (Kang et al., 2000; Tanguy and Berlemont, 2005).

We are here concerned by the primary break-up of a jet and many topological changes occur (interface pinching or merging, droplet coalescence or secondary break-up). The numerical method must describe the interface motion precisely, handle jump conditions at the interface without artificial smoothing, and respect mass conservation. Thus we develop a 3D code, where interface tracking is performed by a level set method, the ghost fluid method is used to capture accurately sharp discontinuities, and the level set and VOF methods are coupled to ensure mass conservation (Sussman and Puckett, 2000). A projection method is used to solve incompressible Navier–Stokes equations that are coupled to a transport equation for the level set function. Specific care has been devoted to improving simulation capabilities with MPI parallelization. We first recall the level set method, then describe the coupling between the level set and VOF techniques and we briefly present the ghost fluid method. Validation test cases are performed and discussed and results are then presented for the primary break-up of a liquid jet with initial turbulent perturbation on the inflow conditions in order to illustrate the potentialities of the method.

2. Methods

2.1. Level set

Level set methods are based on the use of a continuous function ϕ to describe the interface between two media (Sethian, 1996; Osher and Fedkiw, 2003). That function is defined as the signed distance between any point of the domain and the interface which is thus described by the 0 level curve of that function. Solving a convection equation determines the evolution of the interface in a given velocity field $\vec{\mathbf{V}}$:

$$\frac{\partial \phi}{\partial t} + \vec{\mathbf{V}} \cdot \nabla \phi = 0 \tag{1}$$

Specific care is taken with the discretization method, as discontinuities are often observed in the results. To avoid singularities in the distance function field, we thus use the 5th-order WENO scheme for convective terms.

Geometrical information on the interface, such as normal vector $\vec{\mathbf{N}}$ or curvature κ, is easily obtained through:

$$\vec{\mathbf{N}} = \frac{\nabla \phi}{|\nabla \phi|} \quad \kappa(\phi) = -\nabla \cdot \vec{\mathbf{N}} \tag{2}$$

Some problems may arise when the level set method is carried out; high velocity gradients can produce wide spreading and stretching of the level set, and ϕ will no longer remain a distance function. A redistancing algorithm (Sussman et al., 1998) is thus applied to keep ϕ as the signed distance to the interface. The algorithm is based on the iterative resolution of the following equation:

$$\frac{\partial d}{\partial \tau} = \mathrm{sign}(\phi)(1 - |\nabla \phi|) \quad \text{where} \quad d(x,t,\tau)_{\tau=0} = \phi(x,t) \tag{3}$$

where τ is a fictitious time. We solve Eq. (3) until a steady state is reached, thus close to the exact steady state solution, namely either $\text{sign}(\phi) = 0$, meaning that we are on the droplet interface, or $|\nabla d| = 1$ which mathematically defines a distance function. We then replace $\phi(x,t)$ by $d(x,t,\tau_{\text{steady}})$.

Numerical computation of Eqs. (1) and (3) can induce mass loss in under-resolved regions. This is the main drawback of level set methods, but to improve mass conservation, two main extensions of the method can be developed: the particle level set (Enright et al., 2002) and a coupling between VOF and level set (Sussman and Puckett, 2000; van der Pijl et al., 2005). In jet atomization, the interface becomes very wrinkled and many break-ups are initiated. It thus appears that coupling the level set method with the VOF technique is much better adapted for our purpose than the particle level set method, and it is presented in next section.

2.2. Coupling VOF and level set methods

As mentioned above, mass conservation in level set methods requires the mesh to be refined enough to avoid under-resolved region as much as possible. That is unrealistic in 3D configurations and different strategies have been proposed to overcome this difficulty. Most of them are based on the modification of the reinitialization algorithm by adding a constraint to help in mass conservation (Sussman et al., 1998). A major limitation of these methods is that they are global; when many liquid parcels are generated in the flow these corrections are quite impossible.

We thus chose to use the Bourlioux (1995) and Sussman and Puckett (2000) approach (CLSVOF). The main idea is to benefit from the advantage of each strategy, which is to minimize mass loss through the VOF method and to keep a fine description of the geometrical properties of the interface with the level set method. We recall here the main ideas of the CLSVOF method extensively discussed by Sussman and Puckett (2000) and we describe our numerical technique that retains the original CLSVOF method, but we also keep the redistancing algorithm for the level set. In addition the calculation of the liquid volume fraction is detailed.

To couple the VOF method and the level set method, Sussman and Puckett (2000) first defined the volume fraction F, in a grid cell Ω of the domain, at time t, as a function of the level set ϕ (assuming 2D formalism for simplicity):

$$F(\Omega,t) = \frac{1}{|\Omega|}\int_{\Omega} H(\Phi(x,y,t))\,\mathrm{d}x\,\mathrm{d}y \tag{4}$$

$$\text{where } H \text{ is the Heaviside function: } H(\Phi) = \begin{cases} 1 & \text{if } \Phi > 0 \\ 0 & \text{otherwise} \end{cases} \tag{5}$$

It is impossible to transport the liquid volume fraction on the computational domain without knowing the interface position. But using the level set, the interface can be localized and the liquid volume fraction can be advected without any ambiguity.

2.2.1. How to get the volume fraction with the level set

To transport the liquid volume fraction or to define it from the Level Set function, we first define the interface in the cell $\Omega_{i,j}$ as a straight line in 2D (a plane in 3D). A reconstructed level set $\Phi^R_{i,j}$ is defined by Sussman and Puckett (2000):

$$\Phi^R_{i,j} = a_{i,j}(x - x_i) + b_{i,j}(y - y_j) + c_{i,j} \tag{6}$$

When that equation is normalized such that $(a^2_{i,j} + b^2_{i,j}) = 1$, then $a_{i,j}$ and $b_{i,j}$ are the coordinates of the vector normal to the interface. Thus the coefficients $c_{i,j}$ represent the normal distance from the interface to the points (x_i, y_j).

The coefficients $a_{i,j}$, $b_{i,j}$, $c_{i,j}$ are determined so that $\Phi^R_{i,j}$ is as close as possible to the real value of the level set function ϕ. The following error is thus minimized (Sussman and Puckett, 2000):

$$E_{i,j} = \int_{x_{i-1/2}}^{x_{i+1/2}} \int_{y_{j-1/2}}^{y_{j+1/2}} \delta(\Phi)(\Phi - a_{i,j}(x - x_i) - b_{i,j}(y - y_j) - c_{i,j})^2\,\mathrm{d}x\,\mathrm{d}y \tag{7}$$

Using a nine point stencil, discretization of Eq. (7) reads:

$$E_{i,j} = \sum_{i'=i-1}^{i'=i+1} \sum_{j'=j-1}^{j'=j+1} w_{i'-i,j'-j}\delta_\varepsilon(\Phi_{i',j'})(\Phi_{i',j'} - a_{i,j}(x_{i'} - x_i) - b_{i,j}(y_{j'} - y_j) - c_{i,j})^2 \tag{8}$$

$\delta_\varepsilon(\Phi_{i',j'})$ is a smoothed Dirac distribution with thickness ε ($\varepsilon = \sqrt{2}\,\mathrm{d}x$) and $w_{p,q}$ are weighting factors that are maximal on the cell central point (i,j). Minimizing $E_{i,j}$ leads to the following conditions:

$$\frac{\partial E_{i,j}}{\partial a_{i,j}} = \frac{\partial E_{i,j}}{\partial b_{i,j}} = \frac{\partial E_{i,j}}{\partial c_{i,j}} = 0 \tag{9}$$

Eq. (9) requires solving the following 3×3 linear system (4×4 in 3D):

$$\begin{bmatrix} \sum\sum whX^2 & \sum\sum whXY & \sum\sum whX \\ \sum\sum whXY & \sum\sum whY^2 & \sum\sum whY \\ \sum\sum whX & \sum\sum whY & \sum\sum wh \end{bmatrix} \begin{bmatrix} a_{i,j} \\ b_{i,j} \\ c_{i,j} \end{bmatrix} = \begin{bmatrix} \sum\sum wh\Phi X \\ \sum\sum wh\Phi Y \\ \sum\sum wh\Phi \end{bmatrix} \tag{10}$$

where the following notations are used:

$$\begin{aligned} &\sum\sum \leftrightarrow \sum_{i'=i-1}^{i'=i+1} \sum_{j'=j-1}^{j'=j+1} \\ &wh \leftrightarrow w_{i'-i,j'-j}\delta_\varepsilon(\Phi_{i',j'}) \\ &X \leftrightarrow (x_{i'} - x_i) \\ &Y \leftrightarrow (y_{j'} - y_j) \\ &\Phi \leftrightarrow \Phi_{i,j} \end{aligned} \tag{11}$$

A classical linear algorithm can be used to obtain the coefficients $a_{i,j}, b_{i,j}, c_{i,j}$.

Defining the zero level set in a cell allows the initial liquid volume fraction $F(\Omega_{i,j};\ t = 0)$ to be determined:

$$F_{i,j} = \frac{1}{\mathrm{d}x\,\mathrm{d}y} \int_{x_{i-1/2}}^{x_{i+1/2}} \int_{y_{j-1/2}}^{y_{j+1/2}} H(a_{i,j}(x - x_i) + b_{i,j}(y - y_j) + c_{i,j})\,\mathrm{d}x\,\mathrm{d}y \tag{12}$$

Eq. (12) can be easily estimated with geometrical relations; for example in Fig. 1, it corresponds to the sum of the trapeze area A1 and the rectangle area A2.

Note that in 3D configurations, geometrical relations are a little more complicated. We thus set up a method that calculates the liquid volume fraction by integrating the line equation (or the plane equation in 3D).

Writing the line equation $aX + bY + c = 0$ as $Y = AX + B$, $\int Y$ (normalised by $S = \mathrm{d}x\,\mathrm{d}y$) can be analytically calculated. However, the origin of the coordinate system must be defined first; we choose the point with the smallest coordinates, namely $(x_{i-1/2}, y_{j-1/2})$. We might then modify the signs of the coefficients $a'_{i,j}$ and $b'_{i,j}$,

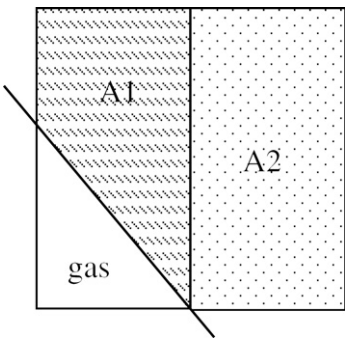

Fig. 1. VOF geometrical scheme.

such that the normal vector to the interface points towards that origin, to ensure that the calculated volume is the liquid volume. Finally we determine the new coefficient $c'_{i,j}$ in order to obtain the line equation $a'(x-x_{i-1/2})+b'(y-y_{j-1/2})+c'=0$. The integral limits are thus the intersection points between the line and the edges of the cell. The scheme is thus:

$$\begin{cases} a_{i,j}(x-x_i)+b_{i,j}(y-y_j)+c_{i,j}=0 \text{ becomes} \\ a'_{i,j}(x-x_{i-1/2})+b'_{i,j}(y-y_{j-1/2})+c'_{i,j}=0 \\ \quad \text{with} \\ a'_{i,j}=-a_{i,j} \quad \text{if } a_{i,j}>0 \\ b'_{i,j}=-b_{i,j} \quad \text{if } b_{i,j}>0 \\ c'_{i,j}=c_{i,j}-(a'_{i,j}0.5\,\mathrm{d}x+b'_{i,j}0.5\,\mathrm{d}y) \end{cases} \tag{13}$$

Going back to the case in Fig. 1, we get (Fig. 2)

$$F_{i,j}=\frac{1}{\mathrm{d}x\,\mathrm{d}y}\left(\left[AX^2+BX\right]_{X_0}^{X_1}+X_0\,\mathrm{d}y\right) \quad \text{with } A=\frac{-a'_{i,j}}{b'_{i,j}} \quad \text{and} \quad B=\frac{-c'_{i,j}}{b'_{i,j}}\,(b_{i,j}\neq 0) \tag{14}$$

If $a_{i,j}$ or $b_{i,j}$ is equal to zero, the line is parallel to one of the axes and no integration is required. This method has been extended to 3D configuration and proves much less difficult to set up than the geometrical approach.

2.2.2. How to correct the level set with the volume fraction

The inverted problem can also be solved, that is the correction of the level set when the liquid volume fraction is known. For any time n, the volume of liquid in a cell must be the same, whatever the method used for its calculation, either from the level set position or from the result of the transport equation for the liquid volume fraction. For a given volume fraction $F^n_{i,j}$, we can write (Sussman and Puckett, 2000)):

$$\frac{1}{\mathrm{d}x\,\mathrm{d}y}\int_{y_{j-1/2}}^{y_{j+1/2}}\int_{x_{i-1/2}}^{x_{i+1/2}} H(a_{i,j}(x-x_i)+b_{i,j}(y-y_j)+c_{i,j})\,\mathrm{d}x\,\mathrm{d}y=F^n_{i,j} \tag{15}$$

where the coefficients $a_{i,j}, b_{i,j}, c_{i,j}$ are given by the zero level set position $\Phi^{n,R}_{i,j}$ at time n. If the equality is not satisfied, a Newton iterative method is applied on the coefficient $c_{i,j}$ (no change on the vector normal to the interface) until a given precision is satisfied for Eq. (15):

$$c^{\mathrm{NEW}}_{i,j}=c_{i,j}-\frac{\left(\frac{1}{\mathrm{d}x\,\mathrm{d}y}\int_{y_{j-1/2}}^{y_{j+1/2}}\int_{x_{i-1/2}}^{x_{i+1/2}}(H(a_{i,j}(x-x_i)+b_{i,j}(y-y_j)+c_{i,j})\,\mathrm{d}x\,\mathrm{d}y)-F^n_{i,j}\right)}{\int_{y_{j-1/2}}^{y_{j+1/2}}\int_{x_{i-1/2}}^{x_{i+1/2}}\delta(a_{i,j}(x-x_i)+b_{i,j}(y-y_j)+c_{i,j})\,\mathrm{d}x\,\mathrm{d}y}\,\mathrm{d}x\,\mathrm{d}y \tag{16}$$

Note that the denominator in Eq. (16) is equal to the length of the zero level set line in the cell (area of the plane in 3D).

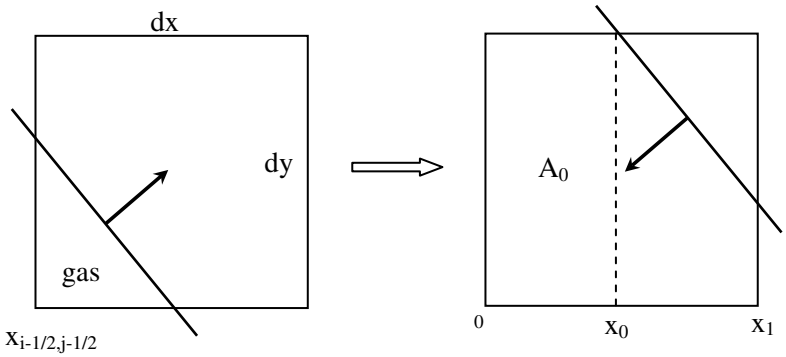

Fig. 2. Change of coordinate system for VOF.

2.3. Coupling the transport of the volume fraction and the level set

The liquid volume fraction is a passive scalar; thus its transport equation is similar to the transport equation (Eq. (1)) of the level set. That equation is discretized following the scheme as defined by Sussman and Puckett (2000); details on the coupled second-order conservative operator split advection are not recalled here. Nevertheless it is important to note that the advection of the liquid volume fraction is carried out with the aid of the zero level set in cells where the interface occurs. The overall algorithm used is now described:

2.3.1. Initialization

Start from a given $\Phi^{n=0}$

- Calculate $a_{i,j}, b_{i,j}, c_{i,j}$ and $\Phi^{R,n=0}_{i,j}$.
- Calculate $F^{n=0}_{i,j}$ (Eq. (12)).

1. Coupled advection of F and Φ
   - Set $\Phi = \Phi^n$.
   - Get $\tilde{F}^n$ and $\widetilde{\Phi}$ with convection of F^n and ϕ in x or y direction (alternately swapped).
   - Calculate $a_{i,j}, b_{i,j}, c_{i,j}$ for $\widetilde{\Phi}^R_{i,j}$.
   - Calculate $c^{\text{new}}_{i,j}$ (Eq. (16)) and $\tilde{\Phi}^R_{i,j}$ for mass conservation.
   - Get $\hat{F}^n$ and $\hat{\Phi}$ with convection of $\tilde{F}^n$ and $\widetilde{\Phi}$ in y or x direction (alternately swapped)
   - Get F^{n+1} and Φ^{n+1} following the operator split algorithm (Sussman and Puckett, 2000).
   - Correction of $F^{n+1}$by setting

     $F^{n+1} = 0 \quad \text{if } F^{n+1} < 0 \text{ or } \Phi^{n+1} < -\Delta x$

     $F^{n+1} = 1 \quad \text{if } F^{n+1} > 1 \text{ or } \Phi^{n+1} > \Delta x$

     $F^{n+1} = F^{n+1} \quad \text{otherwise}$

     to avoid jetsam or flotsam from the VOF transport.
   - Calculate $a_{i,j}, b_{i,j}, c_{i,j}$ and correction of Φ^{n+1}.
   - Get final Φ^{n+1} with the redistancing algorithm, applied for $F^{n+1} = 0$ or $F^{n+1} = 1$ thus no change on the zero level set.
2. Navier–Stokes equation
   - Projection method and then go back to step 1.

2.4. Projection method

The joint level set/VOF method is coupled with a projection method for the direct numerical simulation of incompressible Navier–Stokes equations, expressed as follows:

$$\frac{\partial \vec{\mathbf{V}}}{\partial t} + (\vec{\mathbf{V}} \cdot \nabla)\vec{\mathbf{V}} = -\frac{\nabla p}{\rho} + \frac{\nabla \cdot (2\mu D)}{\rho} + \mathbf{g}$$
$$\nabla \cdot \vec{\mathbf{V}} = 0 \tag{17}$$

where p is the fluid pressure, $\mathbf{g}$ the gravity vector, μ the dynamic viscosity and D is the viscous deformation tensor:

$$\mathbf{D} = 1/2(\nabla \mathbf{V} + \nabla \mathbf{V}^{\mathrm{T}}) \tag{18}$$

In the projection method, the velocity components are expressed on a staggered grid. Spatial derivatives are estimated with a 2nd-order central scheme, but convective terms are approximated by 5th-order WENO scheme discretization in order to ensure a robust behavior of the solution. Temporal derivatives are approximated with the Adams Bashforth algorithm. Poisson equation discretization, with a second order central scheme, leads to a linear system; the system matrix is symmetric and positive definite with five diagonals; a

multigrid algorithm for preconditioning a conjugate gradient method is used (Tanguy and Berlemont, 2005).

2.5. Ghost fluid method

The interface is defined by two different phases and all discontinuities must be carefully described. The jump conditions for an inert interface are applied:

$$\begin{aligned} [p]_\Gamma &= \sigma\kappa(\phi) + 2[\mu]_\Gamma(\nabla u\cdot\vec{\mathbf{N}}, \nabla v\cdot\vec{\mathbf{N}}, \nabla w\cdot\vec{\mathbf{N}})\cdot\vec{\mathbf{N}} \\ [\rho]_\Gamma &= \rho_\mathrm{l} - \rho_\mathrm{g} \\ [\mu]_\Gamma &= \mu_\mathrm{l} - \mu_\mathrm{g} \end{aligned} \tag{19}$$

Specific treatment is thus needed to describe the jump conditions numerically. Two different approaches can be used to represent the above conditions, namely the continuum surface force (CSF formulation) or the ghost fluid method (GFM). The CSF approach has been proved to be robust and leads to interesting results, but two main problems can arise. Smoothing the Heaviside function introduces an interface thickness that depends on the mesh size, and thus an uncertainty on the exact location of the interface. To overcome that smoothing, the ghost fluid method, has been developed by Fedkiw et al. (1999). The formalism respects jump discontinuities across the interface, and avoids an interface thickness. Discretization of discontinuous variables is more accurate, and spurious currents in the velocity field are thus much lower than with CSF methods. We have used this procedure to discretize all discontinuous variables, namely density, viscosity, and pressure (Kang et al., 2000).

In the GFM, ghost cells are defined on each side of the interface and appropriate schemes are applied for the jump conditions. As previously mentioned, the distance function ϕ defines the interface, and jump conditions are extrapolated on some nodes on each side of the interface. Following the jump conditions, the discontinued functions are extended continuously and then their derivatives are estimated. Let us consider a variable f, discontinuous across the interface Γ, that defines two domains Ω^- and Ω^+ (subscript i and $i+1$, respectively), such that the jump of f is $[f]_\Gamma = a(x)$.

The f derivative is then expressed in cells which are crossed by the interface by the following:

$$\left.\frac{\partial f}{\partial x}\right|_{i+\frac{1}{2}} = \frac{f_{i+1}-f_i}{\mathrm{d}x} - \frac{a_\Gamma}{\mathrm{d}x}, \quad a_\Gamma = \frac{a_i|\phi_{i+1}| + a_{i+1}|\phi_i|}{|\phi_i| + |\phi_{i+1}|} \tag{20}$$

and ghost values f^-_{i+1} in Ω^- and f^+_i in Ω^+ are defined by

$$\begin{aligned} f^-_{i+1} &= f^-_{i+1} - a_\Gamma \\ f^+_i &= f^+_i + a_\Gamma \end{aligned} \tag{21}$$

The method is applied for any kind of discontinuities, with the assumption that the interface can be localized inside a grid mesh and that the jumps of the discontinuous variables are known. More details can be found in Liu et al. (2000) on implementing the ghost fluid method to solve the Poisson equation with discontinuous coefficients and on obtaining a solution with jump conditions.

All the simulations are thus carried out with the coupling between level set–VOF–ghost fluid methods. Numerical codes have been developed for 2D and 3D geometries, and specific care has been devoted to improving computing time with MPI parallelization.

3. Improving the level set–VOF coupling

In order to validate our numerical code, the first test case concerns the Rider and Kothe (1995) configuration on the stretching of a circle in a shear velocity field. The main interest of that particular case is to evaluate how well the method is able to conserve mass and to handle the development of very fine filaments. The size of

the 2D domain is $(1,1)$, the mesh size is 128×128, the circle diameter is equal to 0.15 and it is centered on $(0.5, 0.75)$. The velocity field is given by

$$\begin{aligned} \psi &= \frac{1}{\pi}\sin^2(\pi x)\sin^2(\pi y) \\ u &= -\frac{\partial \psi}{\partial y} \\ v &= \frac{\partial \psi}{\partial x} \end{aligned} \tag{22}$$

Fig. 3a presents the interface at times $t = 3$ s; the velocity field is then inverted and Fig. 3b presents the interface for $t = 6$ s. We estimated the mass conservation and less than 0.01% loss is obtained. However the results for the interface shape are not acceptable. We observed that the nine-point stencil that we used for the interface localization fails when two interface fronts are crossing the stencil domain, as it is presented in Figs. 4a and 4b. It is clearly observed in Figs. 4c and 4d that a six-point or a four-point stencil is more suitable in this particular case; thus, that correction is introduced into our numerical method.

The exact solution from Rider and Kothe (1995) is obtained with a Lagrangian method (Fig. 5a) and we present four simulations in Fig. 5b–e. We first observe that coupling the level set method and the VOF method

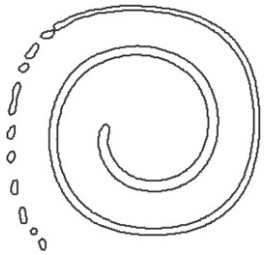

Fig. 3a. Nine point stencil $t = 3$ s.

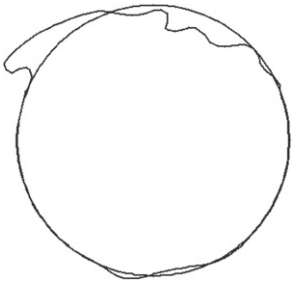

Fig. 3b. Nine point stencil $t = 6$ s.

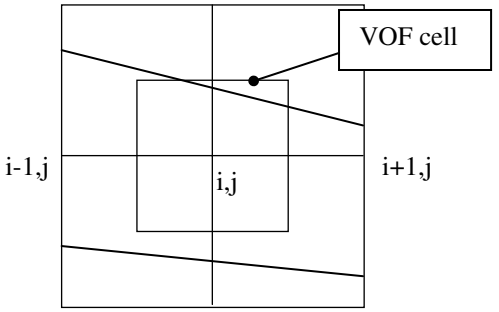

Fig. 4a. Two interfaces in the stencil.

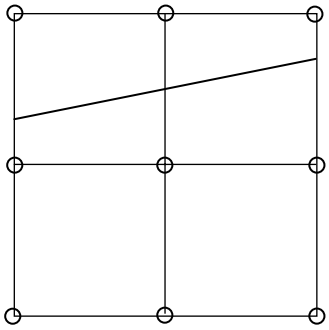

Fig. 4b. Interface reconstruction with a nine-point stencil.

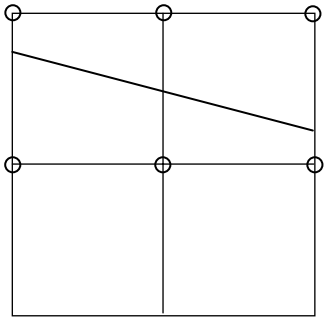

Fig. 4c. Interface reconstruction with a six-point stencil.

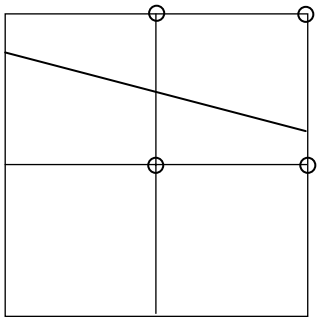

Fig. 4d. Interface reconstruction with a four-point stencil.

greatly improves mass conservation. As expected, mass loss is less than 0.04% on the 128×128 grid and it is less than 0.015% on the finest grid. By comparing Figs. 3a and 5d we can also conclude that the above correction on the number of points in the stencil when two interface fronts are in the stencil domain is very impressive for the capture of fine filaments. Moreover, the results in Fig. 5d and e are very close to the exact solution in Fig. 5a.

A similar test case can be run in 3D configuration. LeVeque (1996) proposed to follow a sphere in a three dimensional velocity field, given by

$$\begin{aligned} u(x,y,z,t) &= 2\sin^2(\pi x)\sin(2\pi y)\sin(2\pi z)\cos(\pi t/3) \\ v(x,y,z,t) &= -\sin(2\pi x)\sin^2(\pi y)\sin(2\pi z)\cos(\pi t/3) \\ w(x,y,z,t) &= -\sin(2\pi x)\sin(2\pi y)\sin^2(\pi z)\cos(\pi t/3) \end{aligned} \tag{23}$$

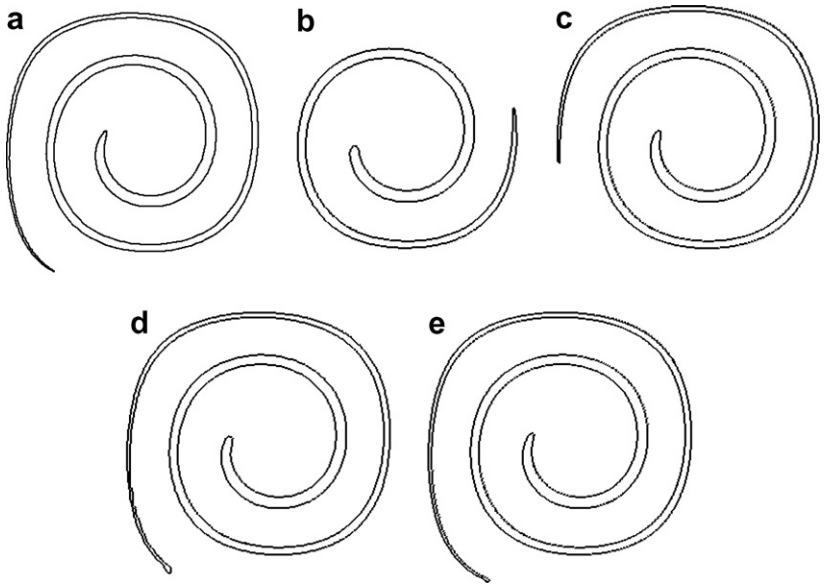

Fig. 5. Level set–VOF with stencil correction: (a) 128×128 exact solution, Lagrangian method ($t = 3$ s); (b) 128×128 level set; (c): 256×256 level set; (d) 128×128; (e) 256×256.

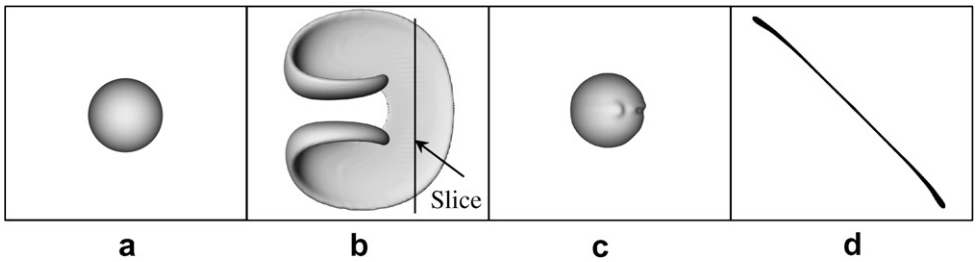

Fig. 6. Deformation of a sphere: VOF/level set method on a 150×150 grid: (a) initial sphere; (b) deformation at $t = 1.5$ s; (c) return to initial position $t = 3$ s; (d) slice of the thin membrane at $t = 1.5$ s.

The domain size is $(1, 1, 1)$ and the grid size is $150 \times 150 \times 150$. The sphere radius is equal to 0.15 and is centered on $(0.35, 0.35, 0.35)$. Note that a reverse motion is applied on the sphere at $t = 1.5$ s. As also mentioned by Enright et al. (2002), we observed more than 50% mass loss with the classical level set method. This test case thus appears well adapted to evaluating our 3D coupling between the level set method and the VOF technique. We present in Fig. 6a–c the results of our simulation for the sphere interface at $t = 0$ s, 1.5 s, and 3.0 s, respectively. Slight deviations from the initial sphere geometry are observed at time $t = 3$ s, but a satisfactory behavior of the 3D code is obtained for that quite difficult test case. A slice of the stretched sphere at $t = 1.5$ s is shown in Fig. 6d and it confirms that no holes are observed in the thin membrane. The computed mass loss is less than 0.03% and the efficiency of our VOF/level set coupling is clearly proved. However, our results are not as good as Enright's simulation with the particle level set method. The slight deformations on the sphere surface at time $t = 3$ s that we observe in our results do not appear in Enright's results. But the particle level set method seems almost impracticable for our purpose, namely the primary break-up of a jet with a large number of liquid packets.

4. Level set–ghost fluid coupling: dispersion diagram of Rayleigh instability

It is well known that the liquid jet break-up can exhibit different behaviors, depending on various parameters. The disintegration of a cylindrical plain jet was studied theoretically by Rayleigh (1878). The jet interface

is unstable under surface tension forces and any disturbance can initiate the growth of a wave along the jet that will lead to its break-up. Following the linear analysis theory, a sinusoidal deformation of the interface is initially imposed:

$$\eta(x, t = 0) = \eta_0 \exp \mathrm{i}kx \tag{24}$$

and propagates along the jet:

$$\eta(x, t) = \eta_0 \exp(wt + \mathrm{i}kx) \tag{25}$$

where x is the streamwise coordinate, t the time, η_0 the initial magnitude of the perturbation, w is the growth rate of the perturbation, and k the wave number ($k = 2\pi/\lambda$).

Noting that the growth rate of the perturbation w is associated with the temporal variable, in this section we consider the temporal stability of capillarity waves. Following Rayleigh's theory, Weber (1931) introduced the liquid viscosity in the instability analysis, and the following dispersion equation is obtained:

$$w^2 F_1 + w F_2 \frac{3\mu\bar{k}^2}{\rho_L a^2} = \frac{\sigma}{2\rho_L a^3}(1 - \bar{k}^2)\bar{k}^2 \quad \text{with } \bar{k} = ka \tag{26}$$

where F1 and F2 are Bessel functions and a is the cylindrical jet radius

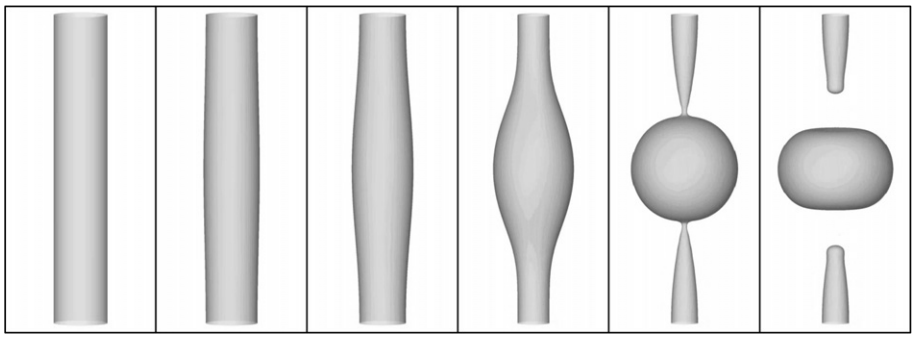

Fig. 7. Rayleigh instability: interface deformation for $\lambda = 4l_r$.

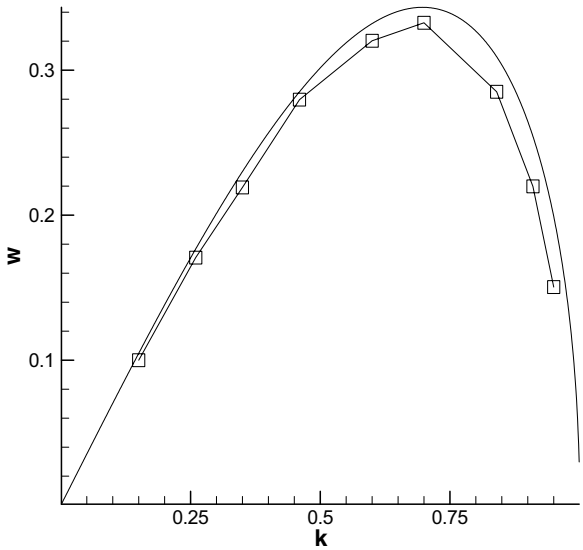

Fig. 8. Rayleigh instability: dispersion diagram; (—) Weber analysis, (□) simulation.

Using Eq. (25), a dispersion diagram is obtained for the growth rate of the perturbation as a function of the initial wave number of the perturbation k.

In the 2D axi-symmetric simulations, the radial length of the domain is $l_r = 10^{-3}$ m, $a = l_r/3$, $l_z = \lambda, k = 2\pi/\lambda$, $\eta_0 = 10^{-4} \cdot \Delta r$, and the initial profile for the level set function is given by

$$\phi(r,z) = a - r + \eta_0 \cos(2\pi z/\lambda) \tag{27}$$

The liquid is water, the gas is air, and the initial velocities are equal to 0. In the radial direction, 61 grid nodes are used, and assuming $\Delta r = \Delta z$, the number of grid nodes in the z-direction is fixed when λ (or k) is given. Periodic boundary conditions are assumed in the direction perpendicular to the jet axis, symmetry is assumed on the jet axis, and a free condition is put on the boundary parallel to the axis. In Fig. 7 we present the time evolution of the interface when $\lambda = 4l_r$.

For each different wave number, the maximum of the growth rate of the perturbation is calculated and the dispersion diagram is presented in Fig. 8. The comparisons between our simulations and the theoretical result from Weber's analysis (Eq. (25)) are satisfactory. This confirms the interest of using the ghost fluid approach, as we did not succeed in getting the same agreement with the continuous force formulation.

5. A first simulation of 3D jet atomization

In order to illustrate how good the level set/VOF/ghost fluid method is for interface tracking, we present a 3D simulation of the primary atomization zone of a turbulent liquid jet. Note that this case is presented here mostly as an illustration of the potentialities of our technique rather than as a reference result.

The main characteristics of the jet are given in Table 1.

Table 1
Jet characteristics

Diameter, D (μm)	Velocity (m s^{-1})	Turbulent intensity	Turbulent length scale
100	100	$u'/U_{liq} = 0.05$	0.1 D
Phase	Density (kg m^{-3})	Viscosity (kg m^{-1}s^{-1})	Surface tension (N m^{-1})
Liquid	696	1.2×10^{-3}	0.06
Gas	25	1×10^{-5}	

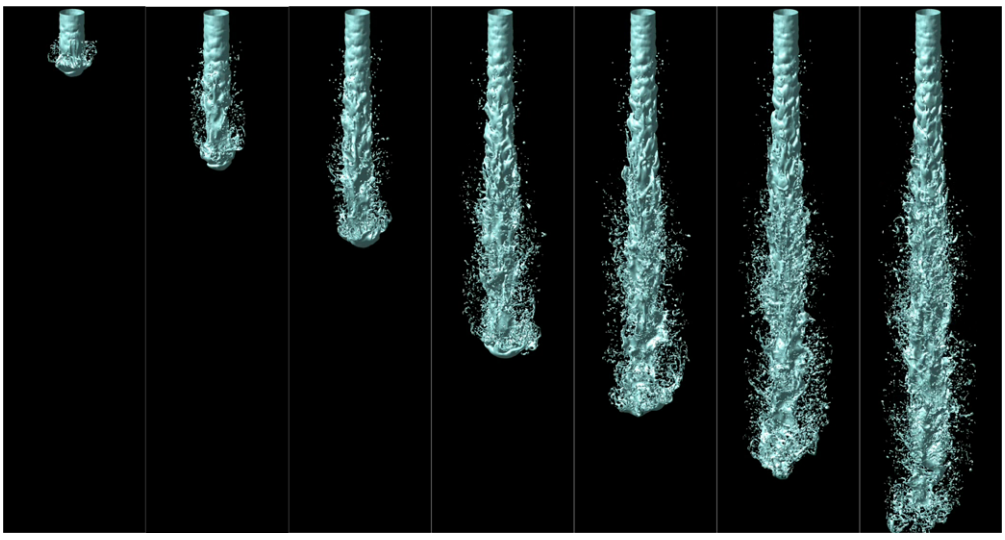

Fig. 9. Development of the liquid jet (time step is 2.5 μm).

The size of the domain is (0.0003, 0.0003, 0.0021) in the (x, y, z) directions. To define the mesh size, we assume that no secondary break up occurs for the smallest droplet. This implies that the Weber number is at least smaller than 10 and gives a minimum droplet diameter equal to 2.4 μm. The uniform grid size is thus set to $128 \times 128 \times 896$, and the grid spacing is 2.36 μm. At injection, the Reynolds number $U_{\mathrm{liq}} D / \nu_{\mathrm{liq}}$ in the liquid is equal to 5800.

Generation of turbulent inflow boundary conditions is still a challenging task when studying the initial development of a jet, with an turbulent inlet perturbation. Here, we use the method derived by Klein et al. (2003), which consists in generating correlated random velocities with a prescribed length scale. In our computation, that scale is taken as the turbulent integral scale L_{t} of a cylindrical channel flow ($L_{\mathrm{t}} = 0.1\mathrm{D}$). With the above mesh size, it corresponds to four times the grid mesh. The turbulence intensity is equal to 0.05 of the mean inlet velocity. The turbulent Reynolds number at injection, based on velocity fluctuations and length scale $u' L_{\mathrm{t}} / \nu_{\mathrm{liq}}$, is equal to 29.

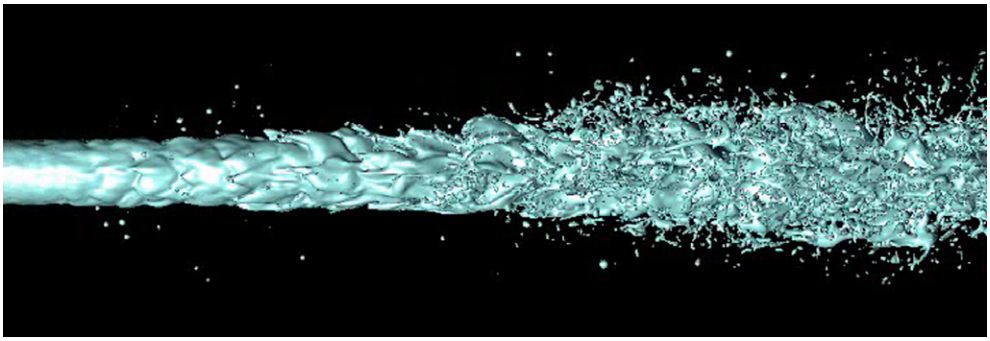

Fig. 10. Liquid jet surface and break-up near the jet nozzle.

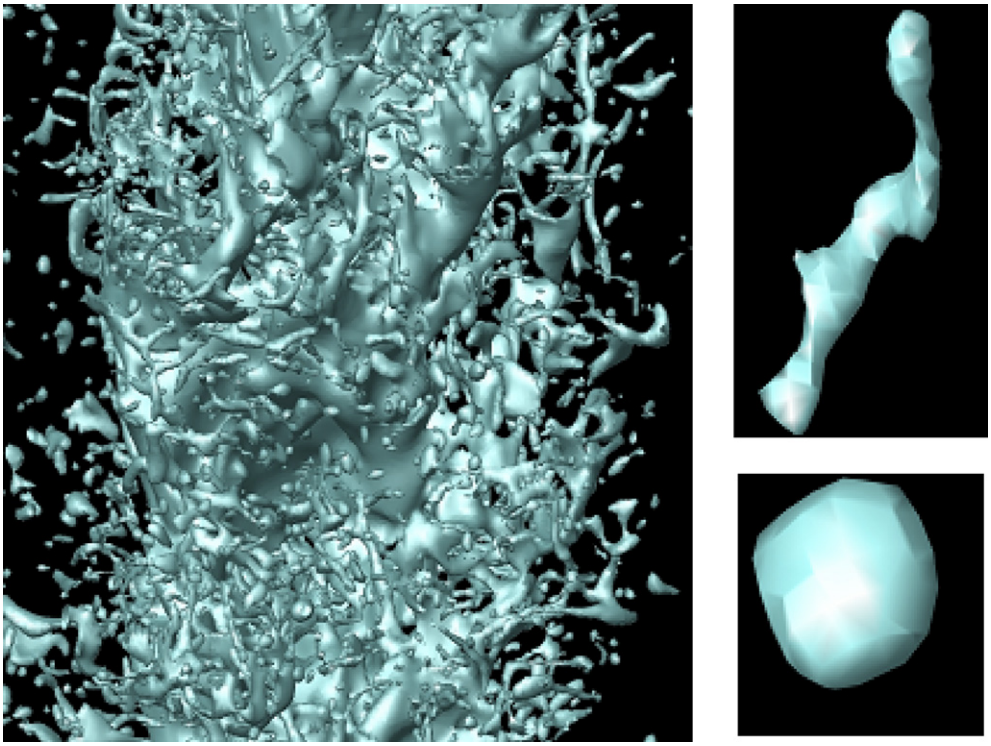

Fig. 11. Liquid parcels.

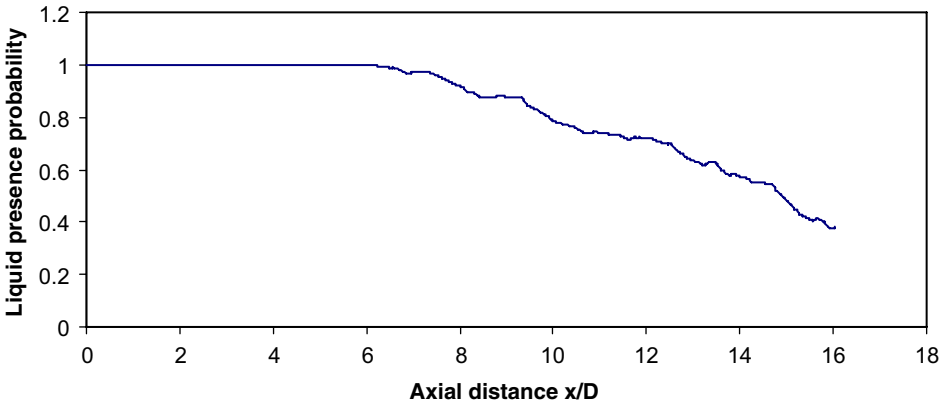

Fig. 12. Liquid presence probability from the level set function on the axis.

The development of the jet is presented on the image sequence (Fig. 9) and the liquid jet surface and break-up near the jet nozzle is presented in Fig. 10. We observe that the first droplets are generated through the break-up at the front of the jet (mushroom shape). The main liquid core is thus surrounded by a cloud of small droplets.

It also appears that 3D waves on the jet interface occur very close to the jet exit. These surface instabilities are of great importance in the liquid atomization. As we observe in Fig. 11, pinching of the interface can produce liquid filaments which then break into droplets, or various liquid packets of different sizes. Moreover, the liquid core appears very tortuous. A liquid presence probability in a mesh is obtained by extracting the continuous part of the liquid from the Level Set function and by carrying out statistics on several images. We present on Fig. 12 the liquid presence probability on the axis and we found that the length of the liquid core is around 7 times the jet diameter. Experimental investigation of the primary break-up of a jet is notoriously a very difficult task; validations of any atomization process simulations are thus nearly impossible at the present time. However high-speed photographs of liquid jet atomization (Yon, 2003) show similar behavior, at least qualitatively. New developments are planned, in particular to include compressibility of the gas phase or to check that the droplet diameter distribution, which can be extracted from the simulations, is non-dependent on the grid mesh. The above calculations are probably under-resolved for a fine description of the spray granulometry. However, we think that the grid resolution is fine enough to describe the initial development of the jet instability.

6. Conclusion

One advantage of the level set method is its ability to represent topological changes, both in 2D or 3D geometry, quite naturally. Moreover, the geometrical properties of the interface, such as the normal vector or curvature, are easily obtained through the level set function gradient. To avoid spreading and stretching of the level set, a redistancing algorithm is applied to ensure that the function remains the algebraic distance to the interface. The ghost fluid method is used to avoid the introduction of a fictitious interface thickness and to reduce parasitic currents. The main drawback of the method is possible mass loss in under-resolved regions. We thus developed the coupling of the ghost fluid and VOF/level set methods, in order to benefit from both the precise interface characterization of the GFM and from the mass conservation of VOF.

Coupling the VOF and level set methods has been proved to be very efficient for mass conservation in 2D and 3D test cases. The interest in coupling the level set and ghost fluid methods is confirmed by the good agreement between Weber's analysis and our results for the dispersion diagram on the Rayleigh instability of a liquid jet. The first attempt to simulate jet atomization with a coupled level set–VOF–ghost fluid method has led to quite impressive results and it appears very encouraging. However, it is obvious that strong interactions are required between experimental research and simulations to further investigate the physical processes in the primary break-up of a liquid jet.

Acknowledgements

Simulations were carried out at the CRIHAN (Centre de Ressources Informatiques de Haute Normandie) and the IDRIS (Institut du Développement et des Ressources en Informatique Scientifique). We thank also Ms. D. Moscato for improving the English.

References

Bourlioux, A., 1995, A coupled level-set volume-of-fluid method for tracking material interfaces. In: Proceedings 6th Annual Int. Symp. on Comp. Fluid Dynamics, Lake Tahoe, USA.

Enright, D., Fedkiw, R., Ferziger, J., Mitchell, I., 2002. A hybrid particle level set method for improved interface capturing. J. Comput. Phys. 183, 83–116.

Fedkiw, R., Aslam, T., Merriman, B., Osher, S., 1999. A non-oscillatory Eulerian approach to interfaces in multimaterial flows (the ghost fluid method). J. Comput. Phys. 152, 457–492.

Gueyffier, D., Li, J., Nadim, A., Scardovelli, S., Zaleski, S., 1999. Volume of Fluid interface tracking with smoothed surface stress methods for three-dimensional flows. J. Comput. Phys. 152, 423–456.

Kang, M., Fedkiw, R., Liu, X.D., 2000. A boundary condition capturing method for multiphase incompressible flow. J. Sci. Comput. 15, 323–360.

Klein, R., Sadiki, S., Janicka, T., 2003. A digital filter based generation of inflow data for spatially developing direct numerical or large eddy simulations. J. Comput. Phys. 186, 652–665.

LeVeque, R., 1996. High-resolution conservative algorithms for advection in incompressible flow. SIAM J. Numer. Anal. 33, 627–665.

Liu, X.D., Fedkiw, R., Kang, M., 2000. Boundary condition capturing method for Poisson equation on irregular domains. J. Sci. Phys., 151–178.

Osher, S., Fedkiw, R., 2003. Level set methods and dynamic implicit surfaces. In: Applied Mathematical Sciences, vol. 153. Springer, New York.

Osher, S., Sethian, J.A., 1988. Fronts propagating with curvature-dependent speed: algorithms based on Hamilton–Jacobi formulations. J. Comput. Phys. 79, 12–49.

Rayleigh, Lord, 1878. On the instability of jets. Proc. London Math. Soc. 10, 4.

Rider, W., Kothe, D., 1995 Stretching and tearing interface tracking methods. In: 12th AIAA CFD Conference, 95-1717, AIAA.

Sethian, J.A., 1996. Level Set Methods and Fast Marching Methods. Cambridge University Press.

Sussman, M., Puckett, E.G., 2000. A coupled level set and volume-of-fluid method for computing 3D and axisymmetric incompressible two-phase flows. J. Comput. Phys. 162, 301–337.

Sussman, M., Smereka, P., Osher, S., 1994. A level set approach for computing solutions to incompressible two-phase flow. J. Comput. Phys. 114, 146–159.

Sussman, M., Fatemi, E., Smereka, P., Osher, S., 1998. An improved level set method for incompressible two-phase. Comput. Fluids 27, 663–680.

Tanguy, S., Berlemont, A., 2005. Application of a level set method for simulation of droplet collisions. Int. J. Multiphase Flow 31, 1015–1035.

Unverdi, S.O., Tryggvason, G., 1992. A front-tracking method for viscous, incompressible multi-fluid flows. J. Comput. Phys. 100, 25–37.

van der Pijl, S.P., Segal, A., Vuik, C., Wesseling, P., 2005. A mass-conserving level-set method for modelling of multi-phase flows. Int. J. Numer. Meth. Fluids 47, 339–361.

Weber, C., 1931. Disintegration of liquid jets. Z. Angew. Math. Mech. 11, 136.

Yon, J., 2003. Jet Diesel haute pression en champ proche et lointain: Etude par imagerie. PhD Université de Rouen, France.